Hindawi
Geofluids
Volume 2022, Article ID 1521837, 8 pages
https://doi.org/10.1155/2022/1521837

Research Article

Experimental Study on Gas–Water Relative Permeability Characteristics of Tight Sandstone Reservoir in Ordos Basin

Xiaoxia Ren,[1,2] **Aifen Li**,[3] **and Asadullah Memon**[4]

[1]*School of Science, Qingdao University of Technology, Qingdao 266525, China*
[2]*Shandong Key Laboratory of Oilfield Chemistry, China University of Petroleum (East China), Qingdao 266580, China*
[3]*School of Petroleum Engineering, China University of Petroleum (East China), Qingdao 266580, China*
[4]*Department of Petroleum and Natural Gas Engineering, Mehran University of Engineering and Technology, Jamshoro, 76062 Sindh, Pakistan*

Correspondence should be addressed to Xiaoxia Ren; renxiaoxia1010@163.com

Received 18 February 2022; Accepted 22 May 2022; Published 8 June 2022

Academic Editor: Xiang Zhou

Accurate measurement of relative permeability curve is the basis for evaluating gas reservoir performance. The unsteady-state method could bring significant measurement error for low-permeability cores. However, it is difficult to control the constant gas flow rate in the traditional steady-state method, which obstacles the experimental operation. In this study, an improved steady-state method was proposed. First, the pressure value obtained from the experiment, when the gas permeability no longer changed with the average pressure on the rock core, was set as the testing pressure. Then, the gas was injected under constant pressure, and the water was injected with a constant flow rate. Finally, the relative permeability values of gas and water phases were calculated based on Darcy's law. Comparative analysis of the results of the relative permeability curves under formation pressure and pressure with negligible slip effect indicates that the relative permeability curves are the same in gas and water phases, proving the feasibility of the new method. Further, the results were compared with those of the test method at normal pressure, the water-phase relative permeability showed no significant change, the relative permeability of gas phase was larger, the two-phase flow area became wider, and the irreducible water saturation was lower than that at the normal pressure. This result reflects that pressure does not significantly affect the flow of wetting phase but tremendously influences the nonwetted phase under low pressure. The relationship between relative permeability and water saturation is linear in the semilogarithmic coordinate diagram and can be described by using the following relationship: $\ln\left(k_{rg}/k_{rw}\right) = aS_w + \ln b$. With the decrease in the core permeability, relative permeability curve, and isotonic point moved to the right, irreducible water saturation gradually increased, and residual gas saturation decreased, indicating that the smaller permeability induced a lower gas-phase flow capacity.

1. Introduction

Gas–water relative permeability is of great significance in the industrial research on natural gas. Relative permeability can be obtained by direct measurement, capillary pressure curve, production data analysis, and indirect calculation methods by using the empirical formulas [1, 2]. Over the past decades, various experiments have been developed and conducted to systematically explore the gas–water relative permeability curves [3–6]. Currently, steady-state and unsteady-state methods are commonly used to obtain relative permeability at the laboratory scale [2]. In the steady-state method, two fluids are simultaneously injected into the core, and their permeability is calculated separately, according to Darcy's law [7, 8]. Abaci et al. [9] injected a mixture of gas and liquid into a vertical artificial sandstone column at room temperature and pressure to measure relative permeability of gas and liquid. The results showed that when water saturation decreased slightly, the relative permeability of water decreased sharply, and the relative permeability of the gas phase at irreducible water saturation was higher than that of the water phase at residual gas saturation. Donald et al. [10] improved the fluid saturation test by

X-ray computed tomography (CT) scanning technology under indoor conditions. The calculation formula for the steady-state method was simple, and the saturation could be measured directly based on Darcy's law. However, it was challenging to maintain the constant gas flow rate by conventional methods, which brought errors into the measurement results.

In contrast, in the unsteady-state method, the displacing phase is injected into the saturated core along with the wetting phase [11–13]. Berry et al. [14] conducted a series of constant-velocity unsteady-state gas–liquid displacement tests on four reservoir sandstone cores with similar porosity, permeability, and lithological characteristics under reservoir conditions. For short-core experiments, if the unsteady-state method is used, the dead volume generally accounts for about 33% of the pore volume of the core [15]. Thus, this effect cannot be ignored, significantly impacting data processing.

Furthermore, the effect of pressure was also studied. However, scholars have different opinions on the effects of overlying strata pressure on relative permeability [16, 17]. Some of the early studies in this area was done by Fatt and Mo et al. [18, 19] and Thomas and Ward [20]. They supposed that the overlying strata pressure would not affect the relative permeability of gas and water phases. However, some literature studies indicated that overlying strata pressure significantly affected the gas–water permeability curves for both gas and water phases [19, 21–25]. Some literature studies also reported that pressure significantly affected the nonwetted phase under the overlying pressure; however, it did not significantly affect the wetting phase [26, 27]. This could be attributed to the increase in the overlying strata that binds sand grains tightly together, resulting in a decrease in the pore throat diameter. For a defined water saturation, this results in redistribution of the wetting phase to occupy more pore throats, which indicates that this cannot cause any significant changes in the water-phase relative permeability (e.g., in water-wet sandstone); however, results in more oil flow blockages thus reduce the relative permeability of nonwet phase [28, 29].

The unsteady-state method often provides errors in measuring gas–water relative permeability curve due to volume measurement, and the influence of pressure on gas–water relative permeability is seldom considered in the currently used test methods. Therefore, based on the traditional steady-state method to measure relative permeability, in this study, the steady-state method is improved and modified. Considering the influence of the formation pressure, the relative permeability curve can be measured by the improved steady-state method, during which water is injected at constant flow as gas is injected at constant pressure. The test results at normal pressure were compared with those at formation pressure to verify the feasibility of this method.

2. Materials and Methods

2.1. Experimental Specimens and Conditions. The specimens used in the experiment were obtained from Sulige gas field, Ordos, Inner Mongolia, with a core diameter of 2.5 cm and length of no more than 5.0 cm. The dimensions, porosities, and permeabilities of the core samples are presented in Table 1. The porosity and permeability were tested under N_2 at 25°C. The experimental temperature was set to the formation temperature of 95°C. Water used was prepared according to the components of output crude oil at the mouth of a well after electric dehydration, and it showed the density of 1.025 g·cm^{-3} and the viscosity of 0.334 mPa·s, at 95°C. The components and viscosity of water for experimental use were found to be almost the same as those under the formation conditions, which could avoid plugging damage caused by incompatibility of injected water.

The wettability of all cores was tested by contact angle measurements with the Kruss DSA-100 drop shape analyzer. A photograph was taken using a camera when a drop of water attached to the surface of a solid. The contact angle between the water and the solid was then calculated.

The confining pressure was set as formation, atmospheric, and pressure with negligible slip effect, respectively.

2.2. Experimental Equipment and Process

2.2.1. Experimental Setup. Figure 1 shows the simulated displacement equipment used for providing high temperature and high reservoir pressure in the test. The system mainly includes displacement pump, humidifier, core holder, gas–water separator, and gas–water metering device.

2.2.2. Experimental Process

(a) By testing gas permeability of rock specimens under different backpressures, the pressure value P_N (under which gas permeability does not change with pressure) was obtained

(b) A core saturated with formation water was placed in a core holder at 95°C and the backpressure of P_N. Formation water was passed through the rock specimen at the constant flow rate (q_w). When the system reached stability, the upstream pressure (P_1) was recorded, and water permeability was calculated

(c) Water driven by gas: gas was injected into the core to gradually increase upstream pressure to P_1. Displacement was continued at constant pressure P_1 until no water was produced, and the gas-phase permeability with irreducible water (S_{wc}) was calculated. The core was sealed, with the conditions reduced to laboratory conditions, and then the core was taken out and weighed to calculate the irreducible water saturation of the core

(d) Simultaneous injection of gas and water: the gas pressure was constant P_1, and water was simultaneously injected at a constant flow rate of $q_w/20$. When the system reached pressure equilibrium, the gas flow rate was recorded, and the effective permeability of the water and gas phases was calculated. Then, the core was weighed following the method mentioned in the previous step, and the water saturation was calculated

Table 1: Basic data of core used in gas–water permeability experiment.

Core number	Length/cm	Diameter/cm	Porosity/%	Perm-plug method/($10^{-3}\mu m^2$)	Dry weight/g	Wet weight/g	Saturated water/mL	Contact angle/°
1	4.240	2.540	17.710	1.896	47.920	51.504	3.497	45.05
2	4.058	2.540	13.629	1.024	52.140	54.664	2.462	49.38
3	4.324	2.530	9.473	0.703	52.717	54.463	1.899	37.65
4	4.549	2.533	15.970	0.516	53.614	56.784	3.093	50.36
5	3.380	2.540	8.140	0.360	42.911	44.116	1.176	32.15
6	3.658	2.536	5.132	0.194	47.300	48.112	0.792	40.56
7	3.681	2.540	3.030	0.130	48.262	48.758	0.484	38.21
8	4.424	2.540	6.240	0.090	57.503	58.557	1.028	36.77

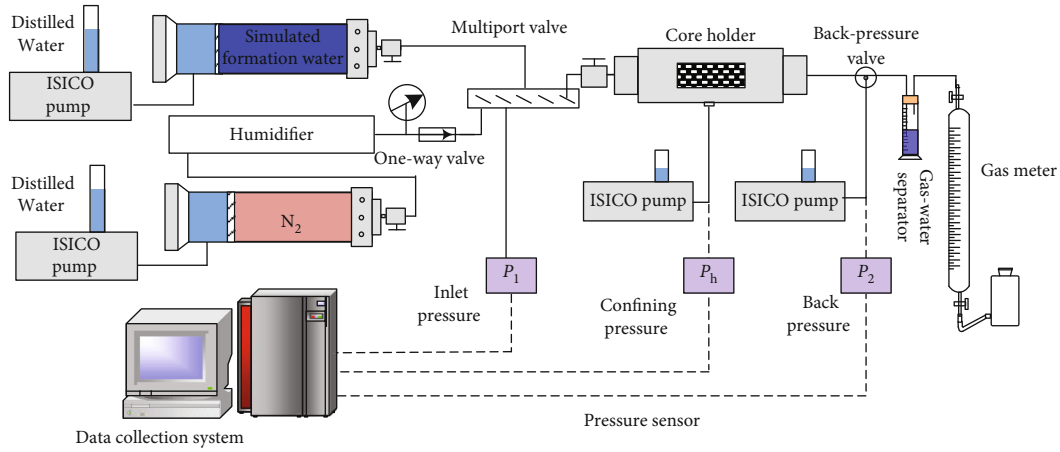

Figure 1: Flow chart of gas–water phase permeability test by the improved steady-state method.

(e) The water flow rate was adjusted to $q_w/10$, and the gas pressure was kept constant P_1. Then, the above-mentioned step d was repeated

(f) The gas source was closed, water was injected with a flow rate of q_w, and then the water-phase relative permeability under residual gas saturation (S_{gr}) was calculated

2.3. Experimental Data Processing Methods. Considering the variation of water and gas volume with temperature and pressure, it is necessary to adjust water and gas production at room temperature and normal pressure to that at high temperature and high pressure. Therefore, the formula for calculating the gas–water-phase permeability curve by a steady-state method was improved as follows:

The volume of liquid under formation conditions is represented as follows:

$$Q_w = Q_{L_0} \cdot B_w, \tag{1}$$

where Q_w denotes the flow rate of water under experimental conditions, $cm^3 \cdot s^{-1}$, Q_{L0} is the flow rate of water under room temperature and normal pressure, $cm^3 \cdot s^{-1}$, and B_w is water volume coefficient under experimental conditions.

Therefore, after reaching stability, according to Darcy's law, liquid-phase permeability is represented as follows:

$$k_w = \frac{Q_{L_0} B_w \mu_w L}{A(p_1 - p_2)}, \tag{2}$$

where k_w is the liquid-phase permeability, cm^2, μ_w denotes water-phase viscosity under experimental conditions, mPa·s, L and A are the core length and cross-section, with the units of cm and cm^2, respectively, and P_1 and P_2 denote upstream and downstream pressure of core holder at steady gas and water discharge, respectively, 10^{-1} MPa.

Figure 2 shows schematic illustration for gas permeability, and Darcy's formula is expressed as follows:

$$Q_g = -\frac{k_g A}{\mu_g} \frac{dp}{dL}, \tag{3}$$

where Q_g is the flow rate of gas under experimental conditions, $cm^3 \cdot s^{-1}$, k_g is the gas permeability, cm^2, μ_g denotes gas viscosity under experimental conditions, mPa·s, A represents core cross-section, cm^2, and dp/dL is the pressure gradient, 10^{-1} MPa·cm^{-1}.

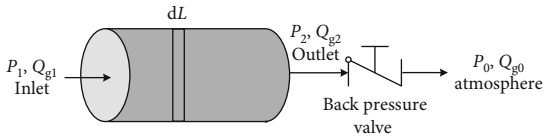

Figure 2: Schematic representation of flow process.

From the gas state formula, on the ground,

$$p_0 Q_{g0} = nRT_0, \tag{4}$$

where p_0 is the atmospheric pressure, 10^{-1} MPa, Q_{g0} is the flow rate of gas under room temperature and normal pressure, $cm^3 \cdot s^{-1}$, n is the amount of substance, mol, R denotes proportionality coefficient, $J \cdot (mol \cdot K)^{-1}$, and T_0 is the room temperature, K.

Under the ground,

$$pQ_g = nz\mathrm{RT}, \tag{5}$$

where p is the experimental mean pressure, 10^{-1} MPa, Q_g is the flow rate of gas under experimental condition, $cm^3 \cdot s^{-1}$, z is the compression factor of gas at experimental temperature and pressure, and T is the experimental temperature, K.

Then,

$$Q_g = \frac{p_0 Q_0 zT}{pT_0} = -\frac{k_g A}{\mu_g}\frac{dp}{dL}. \tag{6}$$

Gas permeability could be obtained by separating the calculus of variations as follows:

$$k_g = \frac{2\mu_g p_0 Q_{g0} zTL}{AT_0\left(p_1^2 - p_2^2\right)}. \tag{7}$$

In this study, the gas-phase permeability under irreducible water is considered as absolute permeability:

$$k_{rg} = \frac{k_g}{k}, \tag{8}$$

$$k_{rw} = \frac{k_w}{k}, \tag{9}$$

where k_{rg} and k_{rw} denote relative permeability of gas and water, respectively, and k is the absolute permeability, cm^2. Average water saturation is as follows:

$$S_w = \frac{m_i - m_o}{V_p \rho_w} B_w, \tag{10}$$

where S_w indicates mean water saturation, m_i and m_0 denote core mass before and after experiment, respectively, g, ρ_w represents density of water at room temperature, $g \cdot cm^{-3}$, and V_p is the pore volume of sample, cm^3.

3. Results and Discussion

3.1. Relation between Gas Permeability and Average Core Pressure. Average pore pressure could affect core permeability due to the Klinkenberg effect [2, 30]. Therefore, in this study, the influence of pressure on gas permeability was tested before conducting experiments on relative permeability.

The experimental results show that gas permeability first decreased rapidly with the increase of average pore pressure and then decreased slowly with the further increase of the pressure. When a specific pressure was reached, there was no significant change in permeability, even with the continuous increase in the pressure. Figure 3 shows that when the average pressure reached 4.25 MPa, the change in permeability became negligible. Therefore, it is reasonable to set backpressure of 5.0 MPa to eliminate slippage effect for gas–water relative permeability test, which is closer to formation conditions.

3.2. Comparison of Gas–Water Phase Permeability Curves under Different Backpressures. In order to verify the effectiveness of this method, experiments were conducted on the relative permeability of core 7 under different backpressure conditions, as shown in Figure 4. The results reveal that there is no significant difference among the three curves for the water phase, which indicates that pressure has no apparent influence on water-phase relative permeability. Noteworthy, relative permeability curves at the backpressure of 5 and 28 MPa are the same in gas and water phases, thus proving the feasibility of the new method. Compared with the gas-phase relative permeability curve under normal pressure, the two-phase penetration area increased, the gas-phase relative permeability became slightly larger, and the irreducible water saturation was lower than that at the normal pressure, which shows that pressure significantly influences gas-phase relative permeability at low pressure.

The improved method can provide the accurate gas–water permeability under the condition of lower pressure than the actual reservoir pressure, which is of great significance to design development scheme for tight gas reservoir, and for the prediction of production performance and reservoir simulation.

3.2.1. Effects of Different Permeabilities on Gas–Water Permeability Curve. Figure 5 shows the test results of the gas–water permeability curve of core No. 4. With the increase of water saturation, the gas-phase relative permeability shows the variation trend of first decreasing rapidly and then decreasing slowly, while the water-phase relative permeability first increases slowly and then rapidly. The gas–water two-phase penetration area of the low-permeability core was relatively narrow, with irreducible water saturation of 63.69% and residual gas saturation of 14.95%. The water saturation corresponding to the isotonic point was higher (about 78%), while the gas–water-phase relative permeability at the isotonic point was lower, about 0.12.

Figure 6 shows gas–water permeability curves of three cores with different permeabilities. The changing trend of the gas–water permeability curve was the same for conditions with different core permeabilities, and the characteristic parameters

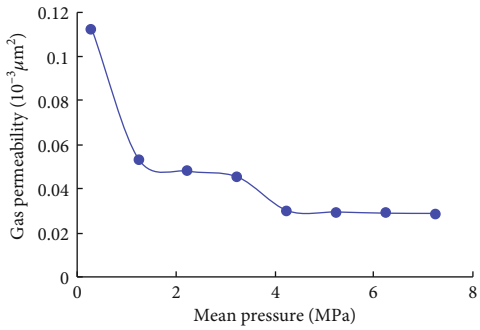

Figure 3: Change of gas permeability with test pressure.

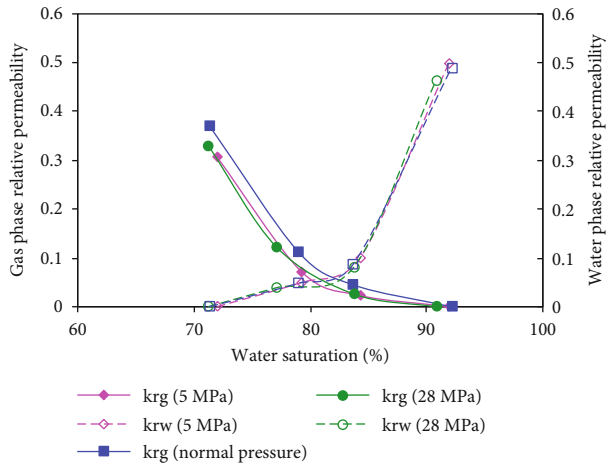

Figure 4: Influence of pressure on gas–water relative permeability curves.

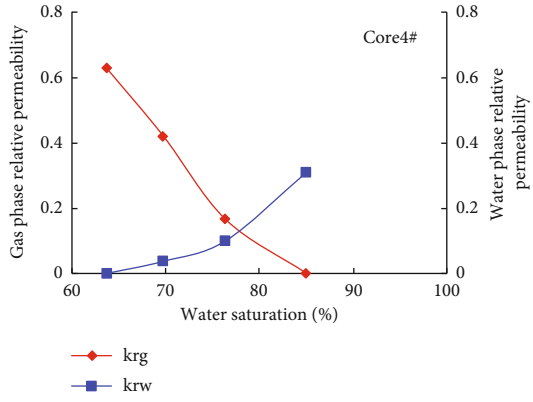

Figure 5: Results of the gas–water permeability curve of core No. 4.

of the gas–water permeability curve changed significantly. The gas-phase permeability curve moved to the right in the same coordinate system with the decrease in permeability. The irreducible water saturation increased, the residual gas saturation decreased, the isotonic point moved to the right, and the two-phase region narrowed. At low permeability, the water-phase relative permeability at residual gas saturation increased compared to gas-phase relative permeability at irreducible water saturation [30, 31].

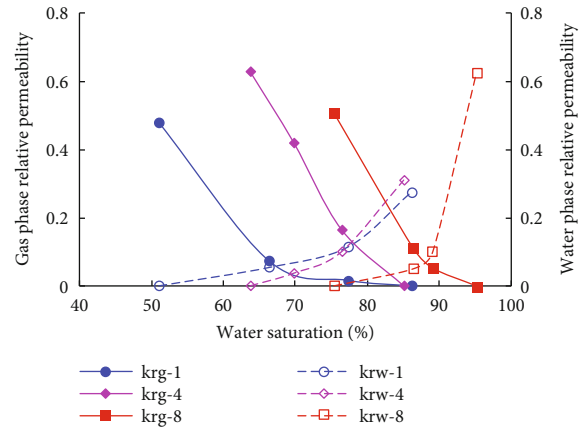

Figure 6: Gas–water permeability curves of cores with different permeabilities.

X-ray analysis results show that the average clay content of cores with a permeability greater than 0.13 mD was 14%, and that of cores with permeability less than 0.13 mD was 8%. Clay minerals are susceptible to speed sensitivity. The gas flow rate was higher than that of water; thus, gas was more susceptible to speed sensitivity when passed through the pores. Moreover, clay content in low permeability core was high; thus, it was easy for the clay minerals to plug the pores, which led to the decrease of gas permeability.

The characteristic parameters for gas–water relative permeability of cores with different permeabilities are listed in Table 2, and the results are presented in Figure 7.

Figure 7(a) exhibits that the irreducible water saturation increases, and residual gas saturation decreases with the decrease in permeability. Notably, all rocks are hydrophilic; therefore, water is the wetting phase, and gas is the nonwetting phase. Before the test, rock was saturated with water, and thus water occupied all pores and throats. When the gas entered the pores under external pressure, the gas could only overcome the capillary force and enter the main pore throat because of the preoccupation of all the percolating channels with water. The smaller the rock permeability, the fewer the larger pore throats. When water reentered the core and displaced the gas, the gas in the mainstream channel could be easily carried away with only a small amount left. Therefore, the smaller permeability induces minor residual gas saturation.

The two-phase flow area narrowed with the decrease in the core permeability (Figure 7(b)). The two-phase flow area reflects the flowability of two-phase fluid in the pore. The decrease of the two-phase flow area indicated a decrease in pore size and poor pore connectivity. Figure 7(b) demonstrates that the water-phase relative permeability under residual gas saturation tends to increase gradually with the decrease of rock permeability. When core permeability was below $0.13 \times 10^{-3}\mu m^2$, the water-phase relative permeability at residual gas saturation was higher than gas-phase relative permeability at irreducible water saturation. This indicates that the lower permeability induces an increased influence of irreducible water saturation on gas permeability.

Table 2: Experiments results of the core samples.

Core No.	$k_g/10^{-3}\mu m^2$	S_{wc}	S_{gr}	Absolute permeability k_g $(S_{wc})/10^{-3}\mu m^2$	k_{rw} (S_{gr})	Two-phase flow range
1	1.896	0.510	0.139	0.480	0.275	0.351
2	1.024	0.531	0.159	0.977	0.525	0.310
3	0.703	0.625	0.135	0.813	0.783	0.240
4	0.516	0.637	0.150	0.629	0.310	0.214
5	0.360	0.656	0.082	0.921	0.966	0.261
6	0.194	0.706	0.031	0.924	0.573	0.264
7	0.130	0.720	0.081	0.307	1.629	0.200
8	0.090	0.753	0.048	0.508	0.625	0.198

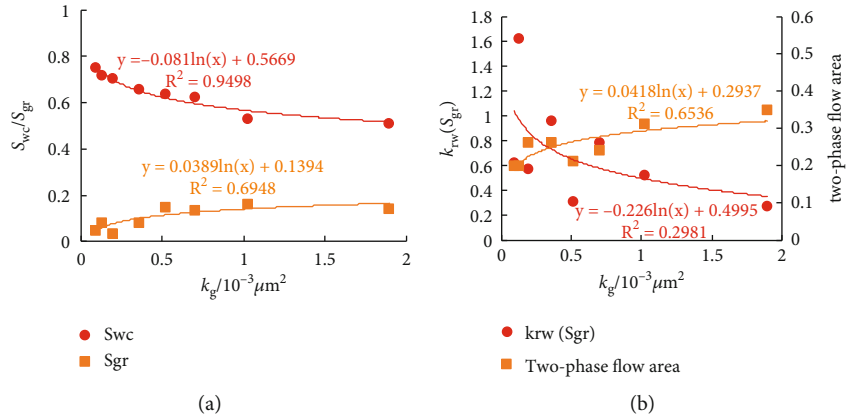

Figure 7: Relationship between characteristic value and permeability of gas–water relative permeability curves: (a) relationship between S_{wc}/S_{gr} and k_g and (b) relationship between k_{rw} (S_{gr})/two-phase flow area and k_g.

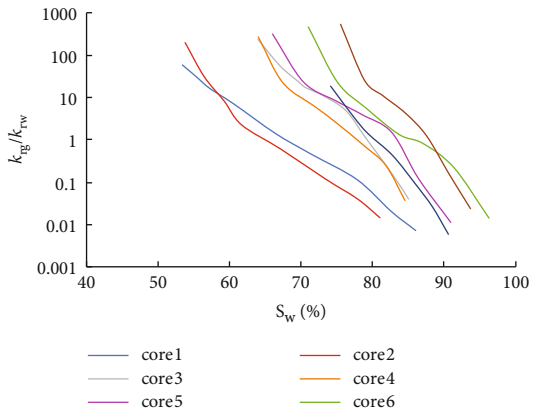

Figure 8: Relationship between k_{rg}/k_{rw} and S_w of cores with different permeabilities.

The relationship between relative permeability and water saturation is shown in Figure 8. Clearly, the curve is linear in the semilogarithmic coordinate diagram and can be described by the relation $\ln(k_{rg}/k_{rw}) = aS_w + \ln b$, where a and b are constants [32–34]. With the increase of water saturation, the relative permeability ratio of the gas–water phase decreases exponentially. When the ratio is 1, the corresponding saturation is the water saturation at the isotonic point. Moreover, the core permeability decreases, and the isotonic point moves to the right. Further, the slope of the eight curves is higher, which indicates that the relative permeability ratio of gas to water decreases rapidly, and the gas-phase permeability is poor. The slope increases gradually with the decrease of permeability, indicating that the smaller permeability induces a lower gas-phase flow capacity.

4. Conclusions

(1) By changing the simultaneous gas–water constant velocity injection mode to gas constant pressure injection and liquid constant flow injection, respectively, an improved steady-state method for determining the gas–water relative permeability of low-permeability sandstones was proposed in this study. This method simulates the formation temperature and determines the backpressure value when the gas permeability no longer changes with the average pore pressure. With this pressure value considered as backpressure, gas was injected at constant pressure, water was injected at constant flow, and relative permeability was calculated by using Darcy's formula. Notably, this method could avoid the errors caused by volume measurement in the unsteady-state method and the errors caused by inaccurate control of gas flow rate in the traditional steady-state method

(2) There was no obvious difference between the gas water relative permeability curve measured by this method and that under formation conditions. Compared with the test method at normal pressure, the relative permeability of the water phase did not exhibit any significant change, the gas-phase relative permeability was larger, and the two-phase flow area was wider, which indicates that pressure significantly influences gas-phase relative permeability at low pressure

(3) With the decrease in the core permeability, relative permeability curve, and isotonic point moved to the right, irreducible water saturation gradually increased, and residual gas saturation decreased. When core permeability was below 0.13 mD, the water-phase relative permeability under residual gas saturation was higher than the gas-phase relative permeability at irreducible water saturation

Data Availability

The data used to support the findings of this study are available from the first author upon request.

Conflicts of Interest

The authors declare that there are no conflicts of interest regarding the publication of this paper.

Acknowledgments

This work was supported by the National Natural Science Foundation of China (NSFC) 52104026.

References

[1] S. Chen, J. Zhang, D. Yin, X. Cheng, and N. Jiang, "Relative permeability measurement of coal microchannels using advanced microchip technology," *Fuel*, vol. 312, Article ID 122633, p. 122633, 2022.

[2] A. Li, *Petrophysics*, China University of Petroleum Press, Dongying, 2015.

[3] J. Wang, M. Dong, and J. Yao, "Calculation of relative permeability in reservoir engineering using an interacting triangular tube bundle model," *Particuology*, vol. 10, no. 6, pp. 710–721, 2012.

[4] A. J. Babchin, R. Bentsen, B. Faybishenko, and M. B. Geilikman, "On the capillary pressure function in porous media based on relative permeabilities of two immiscible fluids: application of capillary bundle models and validation using experimental data," *Advances in Colloid and Interface Science*, vol. 233, no. 462, pp. 176–185, 2016.

[5] B. Xiao, J. Fang, and F. Ding, "Prediction of relative permeability of unsaturated porous media based on fractal theory and Monte Carlo simulation," *Energy & Fuels*, vol. 26, no. 11, pp. 6971–6978, 2012.

[6] N. Zhang, B. Yan, Q. Sun, and Y. Wang, "Improving multiscale mixed finite element method for flow simulation in highly heterogeneous reservoir using adaptivity," *Journal of Petroleum ence & Engineering*, vol. 154, pp. 382–388, 2017.

[7] Y. Wu, K. Pruess, and Z. Chen, "Buckley-Leverett flow in composite porous media," *SPE Advanced Technology Series*, vol. 1, no. 2, pp. 36–42, 1993.

[8] A. Afanasyev, "Fluid displacement in a dual-permeability medium with local capillary equilibrium," *Transport in Porous Media*, vol. 135, no. 2, pp. 513–533, 2020.

[9] S. Abaci, J. Edwards, and B. Whittaker, "Relative permeability measurements for two phase flow in unconsolidated sands," *International Journal of Mine Water*, vol. 11, no. 2, pp. 11–26, 1992.

[10] D. Macallister, K. Miller, S. K. Graham, and C. Yang, "Application of X-ray CT scanning to determine gas/water relative permeabilities," *SPE Formation Evaluation*, vol. 8, no. 3, pp. 184–188, 1993.

[11] D. Dong, "Processing method to the data of relative permeability in unsteady state displacement," *Journal of Southwest Petroleum University Science & Technology Edition*, vol. 36, pp. 110–116, 2014.

[12] X. Ren, A. Li, S. Fu, and S. Wang, "Experimental study on the oil-water relative permeability relationship for tight sandstone considering the nonlinear seepage characteristics," *Journal of Petroleum Science and Engineering*, vol. 161, pp. 409–416, 2018.

[13] X. Chen and D. Dicarlo, "A new unsteady-state method of determining two-phase relative permeability illustrated by CO_2-brine primary drainage in berea sandstone," *Advances in Water Resources*, vol. 96, pp. 251–265, 2016.

[14] F. Berry, A. Little, and R. Skinner, "Differences in gas/oil and gas/water relative permeability," *Proceedings of the SPE/DOE Enhanced Oil Recovery Symposium*, SPE-24133-MS, France, 1992.

[15] W. Hu, S. Yang, G. Liu, Z. Wang, P. Wang, and H. Lei, "A new correction method for oil–water relative permeability curve on the basis of resistivity and water saturation relationship," *Transport in Porous Media*, vol. 109, no. 3, pp. 527–540, 2015.

[16] M. Meng, Z. Qiu, R. Zhong, Z. Liu, Y. Liu, and P. Chen, "Adsorption characteristics of supercritical CO_2/CH_4 on different types of coal and a machine learning approach," *Chemical Engineering Journal*, vol. 368, pp. 847–864, 2019.

[17] M. Meng and Z. Qiu, "Experiment study of mechanical properties and microstructures of bituminous coals influenced by supercritical carbon dioxide," *Fuel*, vol. 219, pp. 223–238, 2018.

[18] I. Fatt, "The effect of overburden pressure on relative permeability," *Journal of Petroleum Technology*, vol. 5, no. 10, pp. 15-16, 1953.

[19] S. Mo, S. He, G. Lei, S. Gai, and Z. Liu, "Effect of the drawdown pressure on the relative permeability in tight gas: a theoretical and experimental study," *Journal of Natural Gas Science and Engineering*, vol. 24, pp. 264–271, 2015.

[20] R. Thomas and D. Ward, "Effect of overburden pressure and water saturation on gas permeability of tight sandstone cores," *Journal of Petroleum Technology*, vol. 24, no. 2, pp. 120–124, 1972.

[21] J. Fang, P. Guo, X. Xiao et al., "Gas-water relative permeability measurement of high temperature and high pressure tight gas reservoirs," *Petroleum Exploration and Development*, vol. 42, no. 1, pp. 92–96, 2015.

[22] X. Guo, Z. Du, Y. Jiang, L. Sun, X. Liu, and N. Zhang, "Can gas-water relative permeability measured under experiment conditions be reliable for the development guidance of a real HPHT

reservoir," *Natural Gas Industry*, vol. 34, no. 6, pp. 60–64, 2014.

[23] S. Mo, S. He, G. Lei, G. Liu, and S. Gai, "Theoretical and experimental analysis of gas-water relative permeability in tight gas," *Natural Gas Geoscience*, vol. 26, no. 11, pp. 2149–2154, 2015.

[24] J. Shen, Y. Qin, Y. Li, and G. Wang, "Experimental investigation into the relative permeability of gas and water in low-rank coal," *Journal of Petroleum Science and Engineering*, vol. 175, pp. 303–316, 2019.

[25] X. Zhang, C. Wu, and S. Liu, "Characteristic analysis and fractal model of the gas-water relative permeability of coal under different confining pressures," *Journal of Petroleum Science and Engineering*, vol. 159, pp. 488–496, 2017.

[26] C. Adenutsi, Z. Li, W. Aggrey, and B. Toro, "Performance of relative permeability and two-phase flow parameters under net effective stress in water wet porous media: a comparative study of water–oil versus silica nanofluid–oil," *Arabian Journal for Science and Engineering*, vol. 43, no. 11, pp. 6555–6565, 2018.

[27] B. Lai and J. Miskimins, "A new technique for accurately measuring two-phase relative permeability under non-Darcy flow conditions," *Journal of Petroleum Science and Engineering*, vol. 127, pp. 398–408, 2015.

[28] L. Wang, Z. Li, C. D. Adenutsi, and C. Wang, "An experimental study of the effect of three metallic oxide nanoparticles on oil-water relative permeability curves derived from the JBN and extended JBN methods," *Journal of Petroleum Science and Engineering*, vol. 233, Article ID 107257, 2020.

[29] H. Sidiq, "UPSCALING gas-water relative permeability measurements from ambient to reservoir CONDITIONS," *Journal of Porous Media*, vol. 22, no. 8, pp. 975–985, 2019.

[30] X. Zhao, Z. Qiu, B. Sun, S. Liu, X. Xing, and M. Wang, "Formation damage mechanisms associated with drilling and completion fluids for deepwater reservoirs," *Journal of Petroleum Science and Engineering*, vol. 173, pp. 112–121, 2019.

[31] L. Shunshe, P. Yuhui, W. Xinshan et al., "Characteristics and classification of gas-water relative permeability curves of tight sandstone reservoirs in Sulige gas field," *Journal of Xi'an Shiyou University(Natural Science Edition)*, vol. 30, no. 6, pp. 55–61+9, 2015.

[32] W. Tian, A. Li, X. Ren, and Y. Josephine, "The threshold pressure gradient effect in the tight sandstone gas reservoirs with high water saturation," *Fuel*, vol. 226, pp. 221–229, 2018.

[33] Y. Guo, H. Liu, A. Gao, Z. Hu, X. Hue, and H. Zhou, "Research and application effect analysis on water-drive characteristic curve for water-drive gas reservoir," *Oil Drilling & Production Technology*, vol. 35, no. 3, pp. 63–65, 2013.

[34] H. Liu, *Principles of Reservoir Engineering*, China University of Petroleum Press, Dongying, China, 2015.